



Since January 2020 Elsevier has created a COVID-19 resource centre with free information in English and Mandarin on the novel coronavirus COVID-19. The COVID-19 resource centre is hosted on Elsevier Connect, the company's public news and information website.

Elsevier hereby grants permission to make all its COVID-19-related research that is available on the COVID-19 resource centre - including this research content - immediately available in PubMed Central and other publicly funded repositories, such as the WHO COVID database with rights for unrestricted research re-use and analyses in any form or by any means with acknowledgement of the original source. These permissions are granted for free by Elsevier for as long as the COVID-19 resource centre remains active.



1,2,3,4,6-Pentagalloyl glucose of *Pistacia lentiscus* can inhibit the replication and transcription processes and viral pathogenesis of SARS-COV-2

Farzaneh Samandar^a, Zeinab Amiri Tehranizadeh^{b,*}, Mohammad Reza Saberi^b, Jamshidkhan Chamani^a

^a Department of Biology, Faculty of Sciences, Mashhad Branch, Islamic Azad University, Mashhad, Iran

^b Department of Medicinal Chemistry, School of Pharmacy, Mashhad University of Medical Sciences, Mashhad, Iran

ARTICLE INFO

Keywords:

SARS-COV-2

1,2,3,4,6-Pentagalloyl glucose

Molecular docking

Molecular Dynamic simulation

PCA

Pistacia sp.

ABSTRACT

SARS-COV-2 stands as the source of the most catastrophic pandemic of this century, known as COVID-19. In this regard, we explored the effects of five *Pistacia* sp. active ingredients on the most crucial targets of SARS-COV-2, including 3CLpro, PLpro, RdRp, helicase, NSP15, and E protein. The results of molecular docking determined 1,2,3,4,6-pentagalloyl glucose (PG) as the most effective compound of *Pistacia* sp, which also confirmed its excellent binding affinities and stable interactions with helicase (−10.76 kcal/mol), RdRp (−10.19 kcal/mol), E protein (−9.51 kcal/mol), and 3CLpro (−9.47 kcal/mol). Furthermore, MD simulation was conducted to investigate the stability of all complexes throughout a 100 ns. In contrast to PLpro and NSP15, the analyses of Lennard-Jones potential, RMSDas, PCA, and SASA verified the ability of PG in forming stable and adequate interactions with RdRp, helicase, 3CLpro, and E protein due to standing as an effective inhibitor among the six targets, these data proposed the capability of PG, the most important compound of *Pistacia* sp., in inducing antiviral, anti-inflammatory, and antioxidant impacts on RdRp, helicase, 3CLpro, and E protein. Therefore, the possibility of inhibiting the replication and transcription processes and viral pathogenesis of SARS-COV-2 may be facilitated through the application of PG.

1. Introduction

As a well-known genus of Anacardiaceae family, *Pistacia* is consisted of about 20 species and can be found across the Mediterranean to Middle Eastern areas. Five species of this genus grow in Iran, including *Pistacia lentiscus* L., *P. Atlantica*, *P. terebinthus* L., *P. vera* L., and *P. khinjuk* Stocks [1–3], which contain the most significant active ingredients of different phytochemical groups such as terpenoids, phenolic compounds, fatty acids, and sterols. Moreover, discoveries claimed the beneficial impacts of every part of these species on many health problems due to their antiviral [4], anti-inflammatory [5–7], antimicrobial [8,9], anti-nociceptive [7], antioxidant [10–12], antitumor [13–15], anticholinesterase [8,16], antidiabetic [17–19], antihyperlipidemic [20], and anti-atherosclerotic qualities [21,22], as well as potential advantages for gastrointestinal disorders [23]. Next to its traditional applications for the treatment of many disorders such as gastroenteritis, liver,

respiratory tract, and urinary management tract, *Pistacia* sp. proved to contain antihypertensive, aphrodisiac, antiseptic, tonic, and antihypertensive properties [1,2,24,25].

As the cause of coronavirus disease 2019 (COVID-19), severe acute respiratory syndrome coronavirus 2 (SARS-CoV-2) led to the most devastating pandemic in recent century. The structure of this virus is composed of an envelope, non-segmented, positive-sense RNA with a length of ~30 kb and codes for several structural proteins such as spike (S) protein [26,27], envelope (E) protein, membrane (M) protein, and nucleocapsid (N) proteins, as well as 16 putative non-structural proteins (NSPs, encoded by replicate complex (orf1ab)) [28–31]. Each protein has a specific role in the virus or the structure of replication cycle. For instance, S protein is responsible for attaching to the host cell receptors and modifying the fusion process [32–34], while E protein is a small integral membrane protein with multiple functions such as virion release, viral pathogenesis, and viral replication cycle [35–37]. Some

* Corresponding author.

E-mail addresses: fa.samandar@gmail.com (F. Samandar), zeinab.amiri86@gmail.com, zeinab.amiri@outlook.com (Z. Amiri Tehranizadeh), SaberiMR@mums.ac.ir (M.R. Saberi), chamani.j@ut.ac.ir (J. Chamani).

<https://doi.org/10.1016/j.mcp.2022.101847>

Received 16 April 2022; Received in revised form 9 July 2022; Accepted 9 July 2022

Available online 14 July 2022

0890-8508/© 2022 Elsevier Ltd. All rights reserved.

Table 1

The molecular docking results for all complexes.

Complex's name	Binding energy (kcal/mol)	Interactions	Distance	E (kcal/mol)
3CLpro-PG	−9.47	GLN 189 H-donor	2.83	−1.1
		THR 24 H-donor	2.85	−1.7
		MET 49 H-donor	3.81	−0.5
		GLY 143 H-acceptor	3.08	−0.8
		THR 25 H-acceptor	3.46	−0.6
		THR 26 H-acceptor	3.16	−2.0
		MET 49 H-donor	4.41	−2.4
3CLpro-Semiprevir	−10.14	MET 49 H-donor	4.12	−0.7
		GLU 166 H-donor	3.78	−0.7
		GLU 166 Ionic	3.78	−1.0
		GLU 166 pi-H	4.59	−0.5
		GLU 167 (D) H-donor	2.83	−5.4
		MET 208 (D) H-donor	4.35	−0.8
		ASP 164 (D) H-donor	3.30	−0.9
PLpro-PG	−8.06	TYR 273 (D) H-acceptor	2.58	−2.8
		TYR 268 (D) H-donor	2.91	−2.4
		GLY 163 (D) H-donor	3.27	−0.5
		GLY 163 (D) H-donor	2.88	−4.7
		GLY 163 (D) H-acceptor	3.22	−2.7
		GLY 271 (D) H-donor	2.81	−3.4
		GLY 271 (D) H-acceptor	3.26	−1.3
PLpro-Vir251	−8.14	TRP 106 (D) H-acceptor	3.02	−2.0
		ASP 760 H-donor	2.88	−5.2
		ARG 553 H-acceptor	3.13	−1.5
		THR 556 H-acceptor	3.24	−0.9
		LYS 545 H-acceptor	2.80	−5.4
		LYS 545 Ionic	2.80	−6.0
		TRP 617 H-donor	3.04	−3.1
RdRp-PG	−10.19	ASP 761 Ionic	3.32	−2.7
		ASP 761 Ionic	3.86	−0.8
		ASP 761 Ionic	3.10	−3.9
		SER 682 pi-H	3.68	−0.5
		GLU 319 H-donor	3.10	−0.6
		ASP 374 H-donor	2.84	−5.4
		ASP 374 H-donor	2.83	−3.8
RdRp-Dabigatran etexilate	−9.41	LYS 320 H-acceptor	2.88	−14.7
		LYS 320 Ionic	2.88	−5.3
		GLU 375 H-donor	3.02	−3.7
		GLU 375 H-donor	3.31	−4.6
		GLU 375 Ionic	3.02	−4.4
		GLU 375 Ionic	3.31	−2.7
		LYS 320 H-acceptor	2.92	−0.7
NSP13-PG	−10.76	HIS 290 H-pi	4.37	−0.5
		GLN 245 (A) H-donor	3.14	−1.7
		GLU 340 (A) H-donor	2.80	−5.3
		ASP 240 (A) H-donor	2.92	−4.9
		THR 341 (A) H-acceptor	3.36	−0.6
		LYS 345 (A) Ionic	3.61	−1.5
		HIS 235 (A) pi-pi	3.48	−0.0
NSP13-Ritonavir	−10.65	—	—	—
		—	—	—
		—	—	—
		—	—	—
		—	—	—
		—	—	—
		—	—	—
NSP15-PG	−8.65	—	—	—
		—	—	—
		—	—	—
		—	—	—
		—	—	—
		—	—	—
		—	—	—
NSP15-Ritonavir	−8.61	—	—	—
		—	—	—
E protein-PG	−9.51	—	—	—
		—	—	—
E protein-Ritonavir	−9.66	—	—	—
		—	—	—

other virus proteins with significant roles in the replication and transcription processes contain two cysteine proteases including the main protease (3CL like protease (3CLpro or Mpro)) and the papain-like protease (PLpro), along with helicase (NSP 13), RNA-dependent RNA polymerase (RdRp), and NSP15 (endoRNase), which can be considered as crucial and vital targets for the inhibition of SARS-COV-2 [31,38,39].

Since the five species of *Pistacia* sp. that can be cultivated in Iran were observed to accommodate particular active ingredients, in this research attempted to probe their effects on the most significant proteins of SARS-COV-2, including 3CLpro, PLpro, RdRp, helicase, NSP15, and E protein, due to their vital functionalities in the pathogenic cycle of virus. The binding affinity of each interaction was calculated and the most ideal practical *Pistacia*'s compound was defined by molecular docking. In addition, we investigated the stability and inhibitory nature of this compound in comparison to the associated inhibitory ligand with each target through the usage of molecular dynamics simulations.

2. Material and method

2.1. Ligands and proteins

The data of previous literature have established the vital and significant functionality of main protease (3CLpro, PDB ID: 6LU7), Papain-like protease (PLpro, PDB ID: 6WX4), RNA-dependent RNA polymerase (RdRp, PDB ID: 6M71), envelope (E) protein (PDB ID: 7k3g), helicase (NSP13, PDB ID: 6ZSL), and endoRNase (NSP15, PDB ID: 6WLC) throughout the viral pathogenic cycle of SARS-COV-2 [40–45]. Therefore, these crucial proteins were selected as the targets of this research. The X-ray crystal structures of each protein were downloaded from Protein Data Bank (www.rcsbPDB.org). Also, the SDF files of three-dimensional structures of the ligands, including all the active ingredients of the five Iranian species of *Pistacia* sp., were procured from the PubChem database (<http://pubchem.ncbi.nlm.nih.gov>).

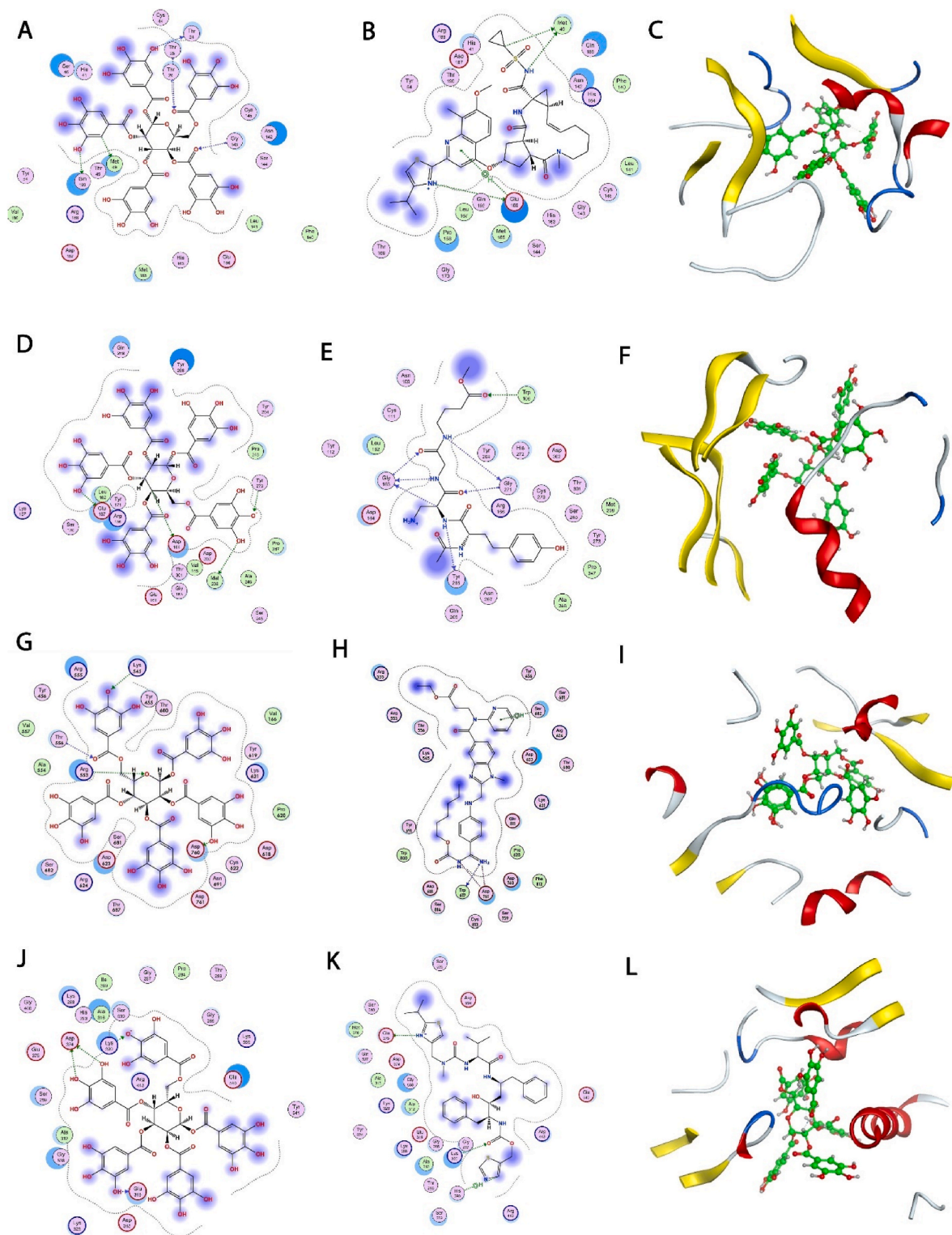


Fig. 1. Molecular docking results of all complexes. (A) 3CLpro-PG complex (B) 3CLpro- Simeprevir complex (C) PG in the 3CLpro's active site (D) PLpro-PG complex (E) PLpro-Vir251 complex (F) PG in the PLpro's active site (G) RdRp-PG complex (H) RdRp- Dabigatran etexilate complex (I) PG in the RdRp's active site (J) helicase-PG complex (K) helicase-Ritonavir complex (L) PG in the helicase's active site. (M) NSP15-PG complex (N) NSP15-Ritonavir complex (O) PG in the NSP15's active site (P) E protein-PG complex (Q) E protein-Ritonavir complex (R) PG in the E protein's active site.

2.2. Molecular docking

The most effective active ingredients of *Pistacia* sp. in interaction with the selected targets were determined by the application of MOE

version 2019 [46]. Initially, we eliminated all the ligands and water molecules from the crystal structures of proteins' PDB files. Then, the MOE-Quick prep tool was used to optimize and prepare the ligands and protein targets for the docking process and modify the breaks or defects

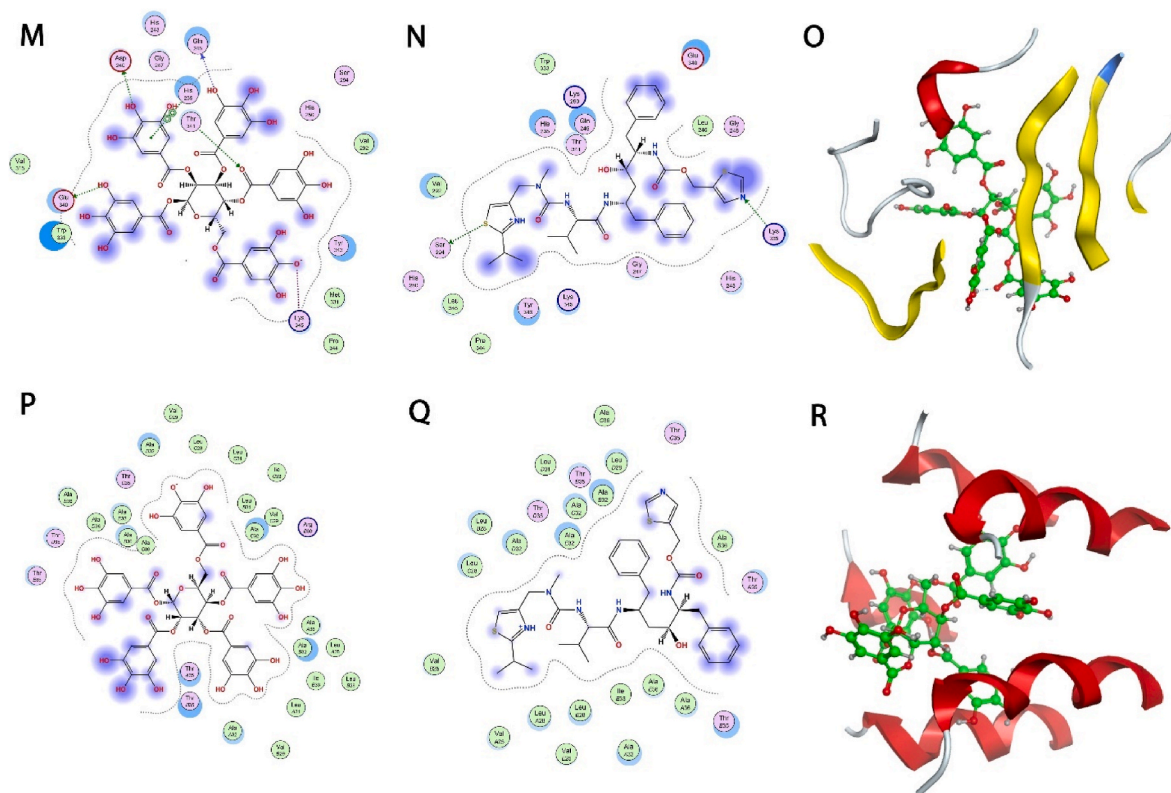


Fig. 1. (continued).

of the protein structure. The last step was to dock the ligands into the selected targets by the MOE-Dock tool in order to report the best interaction through the London Dock scoring function, which involved the calculation of free energy for each hit to score the suitable conformations. Meanwhile, the binding affinities of every complex was estimated through the GBVI/WSA algorithm [47,48].

2.3. Molecular dynamic simulation

The stability and accuracy of protein-ligand complexes were evaluated by the employment of GROMACS version 2018 [49] and CHARMM36 force field [50]. In this section, once the cubic unit cell was defined and filled with explicit water model based on the spc/e, an adequate amount of sodium and chlorine ions were added to neutralize the system. Also, we applied energy minimization in accordance with the Steepest Descent algorithm to eliminate some of the steric clashes between the atoms. NVT and NPT were exerted as the equilibration steps, according to the modified Berendsen thermostat and Parrinello-Rahman, respectively, in prior to the MD simulation to equilibrate the entire system with water and ions [51]. Finally, all of the complexes were subjected to the performance of 100 ns simulation. The capability of selected ligand in inhibiting the targets were investigated through the analyzing processes of PCA, SASA, DSSP, RMSD, RMSF, Rg, and Lennard-Jones potential.

3. Results

3.1. Molecular docking

The conduction of molecular docking facilitated the prediction of the best beneficial ingredients of *Pistacia* sp. in interaction with SARS-COV-2's proteins and also helped in identifying the interaction behavior of our ligands. We docked 40 ingredients of the five Iranian species of *Pistacia* sp. into the 3CLpro, PLpro, RdRp, Helicase (NSP13), endoRNase

(NSP15), and E protein. For each protein target, we performed molecular docking with their inhibitors (up to 10 inhibitors for each target) and compared the best result of each sample with 1,2,3,4,6-pentagalloyl glucose (PG). PG is one of *Pistacia lentiscus*'s ingredients that obtained the best result in interaction with all of the targets. Table 1 exhibits the best docking results of PG and inhibitors. (The docking results of the other ingredients of *Pistacia* sp. are represented in Supplementary information).

The best docking results of ingredients and inhibitors in interaction with 3CLpro was achieved by PG (−9.47 kcal/mol) and Simeprevir (−10.14 kcal/mol), respectively. Based on previous investigations, 3CLpro has three domains with an active site in domain II along with the residues of 140–145 and 163–166 [52]. According to Fig. 1(A–C), PG can be precisely positioned in the active site of 3CLpro and form a stable interaction with this target by creating suitable hydrogen bonds. In contrast to Simeprevir, PG exhibited an adequate and stable performance as an inhibitor.

The binding energies of PG and Vir251 in interaction with PLpro were −8.06 and −8.14 kcal/mol, respectively. The essential residues in PLpro with significant functionalities include CYS111, HIS272, and ASP286 that stand as catalytic triad, as well as and TYR268, MET208, PRO247, PRO248, THR301, TYR264, ASN267, GLN269, LEU162, CYS270, GLY271, and TYR273 that act as substrate-binding residues [53]. In conformity to Fig. 1D–F, PG can be satisfyingly settled in the substrate-binding site and form a stable interaction through the production of hydrogen bonds.

The binding energies of the interaction between RdRp with PG and Dabigatran etexilate, were −10.19 and −9.41 kcal/mol, respectively. Next to the observed active site of RdRp in residues 611 to 626, there were some other principal residues that contained catalytic site (753–767) and NTP entry channel (LYS545, ARG553, ARG555) [52]. As exhibited in Fig. 1G–I, PG produced a stable interaction with the residues of active site and two other chief sites through the formation of appropriate hydrogen bonds and one Ionic bond. In comparison to Dabigatran

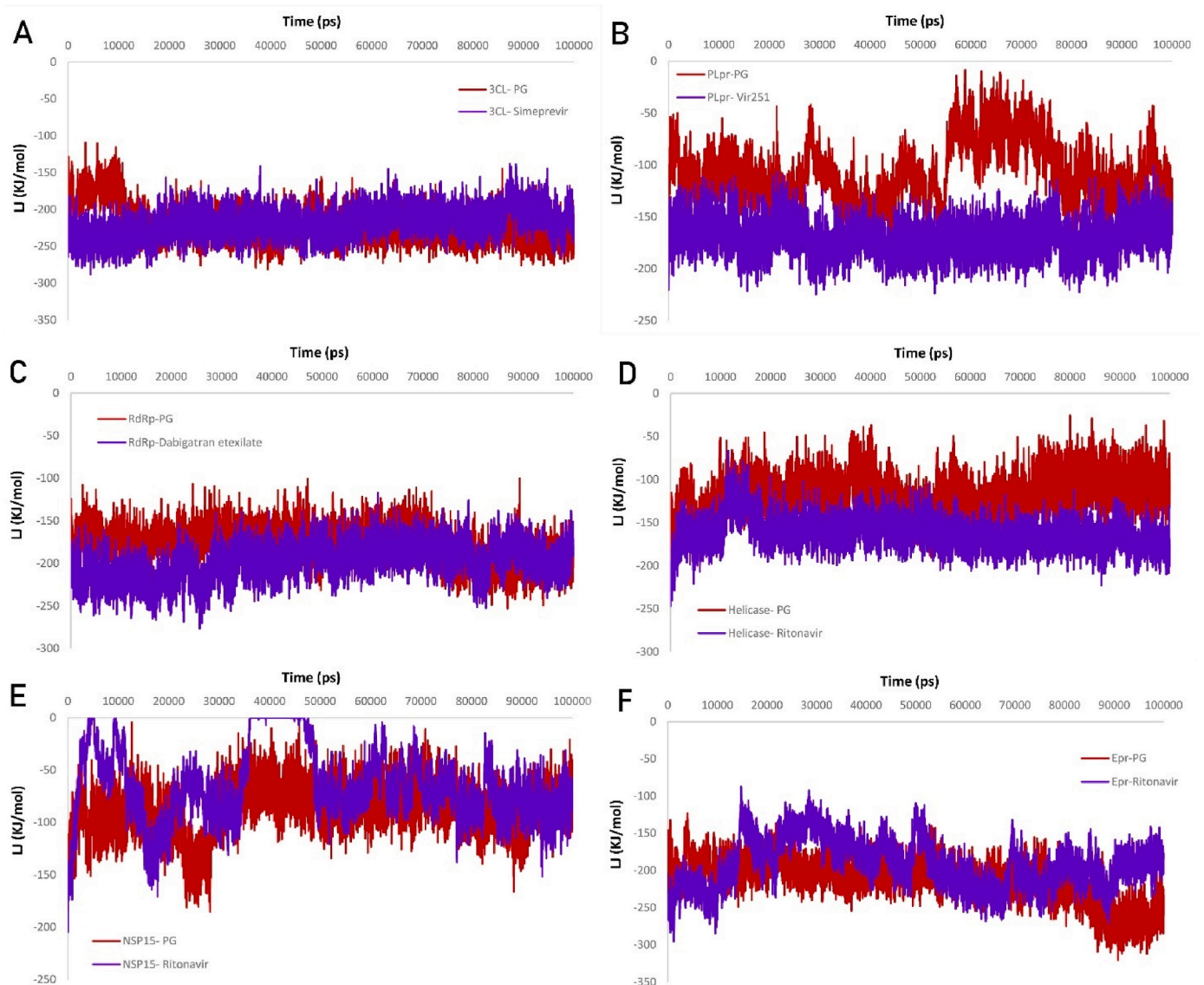


Fig. 2. The plots of Lennard-Jones potential for all interactions. (A) 3CLpro's complexes (B) PLpro's complexes (C) RdRp's complexes (D) helicase's complexes (E) NSP15's complexes (F) E protein's complexes.

etexilate, the higher binding energy of PG can exceed the capability of our ligand in inhibiting RdRp.

The binding energies of PG and Ritonavir in interaction with helicase (NSP13) were -10.76 and -10.65 kcal/mol. Among the four sites of NSP13, site 2 is an ATP binding site located between the 1A and 2A domains while containing six primary residues (LYS288, SER289, ASP374, GLU375, GLN404, and ARG567) [54]. According to Fig. 1J-L, PG can be accurately located in the ATP binding pocket and form a suitable and stable interaction by producing hydrogen and Ionic bonds, which would lead to the inhibition of helicase functionality due to its sufficient interaction with ATP binding site.

The binding energies of NSP15 in complex to PG and Ritonavir were -8.65 and -8.61 kcal/mol, respectively. According to the *in-silico* research, the active site of NSP15 was found in a shallow groove between two anti-parallel β -sheets with six primary catalytic residues including His235, His250, Lys290, Ser294, Thr341, and Tyr343 [55]. Fig. 1M-O displays the precise location of PG in the active site upon its interaction with NSP15, which created a stable interaction by forming hydrogen bonds, Ionic bond, and pi-pi interaction.

The E protein is one of the structural proteins of SARS-COV-2. Residues 8–38 can form the ion-conducting transmembrane (TM) domain

with a N-terminal segment that would contain the residues E8–I13, and a C-terminal segment composed of residues T35–R38 [43]. Relative research proved the possibility of semi-independent interaction of channel's N- and C-terminal with other viral and host proteins. According to the docking results (Fig. 1 (P-R)), the binding energies of PG and Ritonavir were -9.51 and -9.66 kcal/mol, respectively. Table 1 only reports the hydrogen bonds, ionic force, pi-pi, and pi-H interactions between ligands and targets. However, especially in the interaction between E protein with PG and ritonavir, the non-bonded interactions such as hydrophobic force and Lennard-Jones potential could play significant roles in forming stable interactions with this target. Since the gathered data displayed the interaction of PG with C-terminal's residues, it may be capable of disrupting the interaction with host cell proteins and function properly with E protein as a result of interacting with the residues of C-terminal.

3.2. Molecular dynamic simulation

3.2.1. Lennard-Jones potential

Lennard-Jones (LJ) potential is one of the long-range non-bonded interactions and its negative value represents the existence of higher

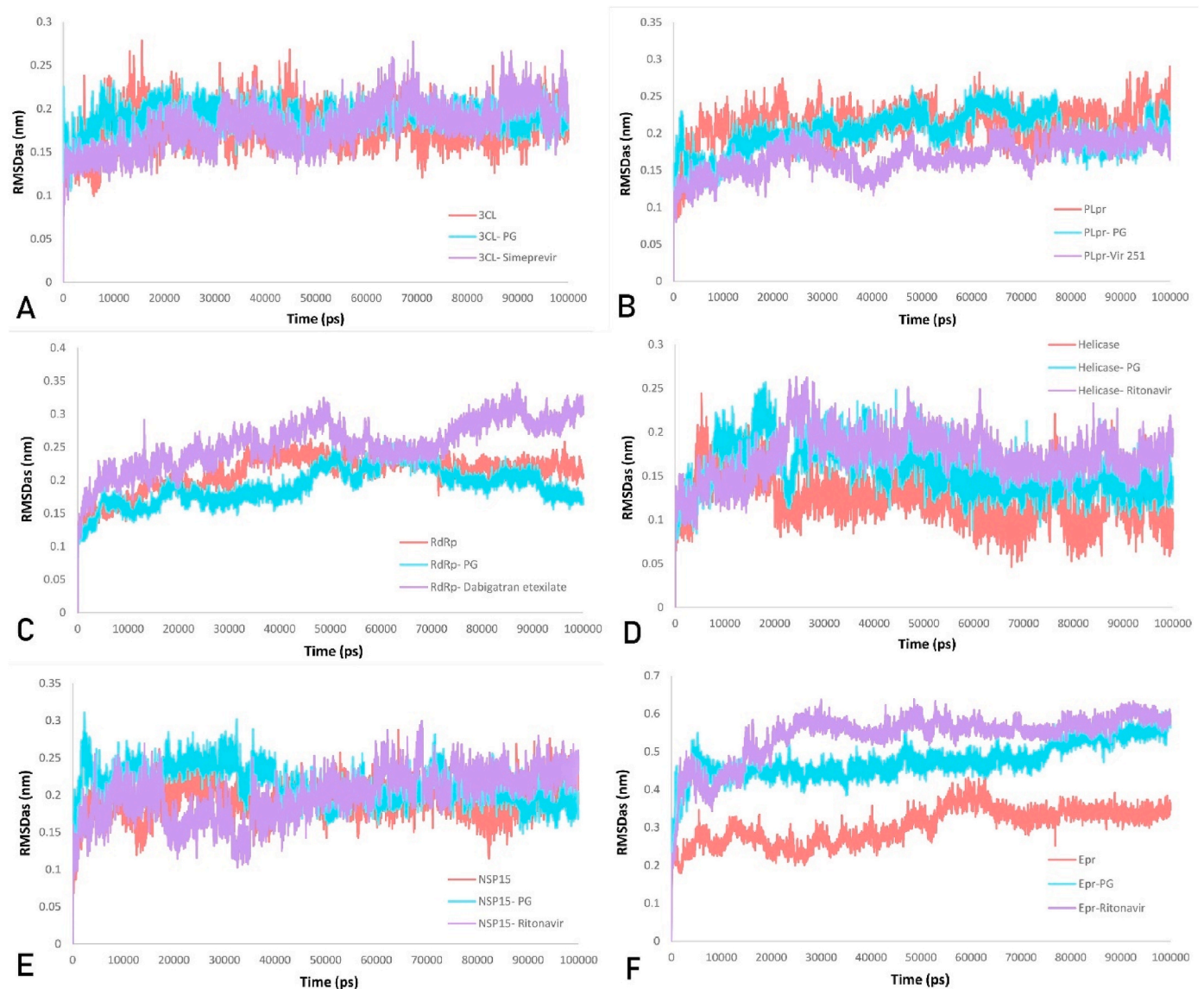


Fig. 3. The plots of RMSDas for all interactions. (A) 3CLpro's complexes (B) PLpro's complexes (C) RdRp's complexes (D) helicase's complexes (E) NSP15's complexes (F) E protein's complexes.

Table 2

The average value of Rg, SASA, and RMSF.

Complexes	Rg (nm)	SASA (nm ²)	RMSF (nm)	
			Protein	Active site
3CLpro	2.24	150.13	0.13	0.14
3CLpro-PG	2.24	151.11	0.12	0.1
3CLpro-Simeprevir	2.23	148.62	0.12	0.11
PLpro	2.5	173.91	0.12	0.107
PLpro-PG	2.5	174.08	0.13	0.114
PLpro-Vir251	2.51	164.87	0.13	0.111
RdRp	3.2	413.82	0.149	0.116
RdRp-PG	3.18	411.61	0.151	0.119
RdRp- Dabigatran etexilate	3.17	405.1	0.154	0.137
Helicase	2.84	291.28	0.169	0.094
Helicase-PG	2.82	284.76	0.164	0.104
Helicase-Ritonavir	2.82	281.25	0.150	0.106
NSP15	2.37	179.54	0.118	0.124
NSP15-PG	2.38	179.55	0.136	0.152
NSP15-Ritonavir	2.37	179.49	0.123	0.138
E protein	1.66	97.42	0.239	0.197
E protein-PG	1.64	97.6	0.194	0.182
E protein-Ritonavir	1.7	94.63	0.225	0.203

attraction and paramount stability. The LJ potential analysis was assessed with a precise grasp of the interaction behavior between ligands and targets.

The average value of LJ potential of PG and Simeprevir in interaction with 3CLpro were -220.583 and -219.389 kJ/mol, respectively. In conformity to Fig. 2A, subsequent to the first 100000 ps, PG displayed minor and constant fluctuations throughout the course of simulation, while containing a higher value of LJ and exhibiting a similar fluctuation to Simeprevir. These results confirmed the capability of PG in forming excellent and firm interaction with 3CLpro as a powerful inhibitor.

The average value of LJ potential of PLpro in complexes to PG and Vir251 were -109.199 and -170.882 kJ/mol, respectively. Fig. 2B exhibits the relatively chief fluctuation rate of PG during the 100 ns along with a lower value of LJ potential when compared to Vir251. Therefore, PG may be incapable of facilitating the specific targeting of PLpro.

The LJ potential value of RdRp in interaction with PG and Dabigatran etexilate were -179.824 and -199.585 kJ/mol, respectively. Next to the lower average value of PG in comparison to inhibitor ligand, it contained a minor and constant fluctuation during the simulation as it is displayed in Fig. 2C. Hence, PG can stand as a suitable inhibitor for RdRp due to creating a stable interaction with this target.

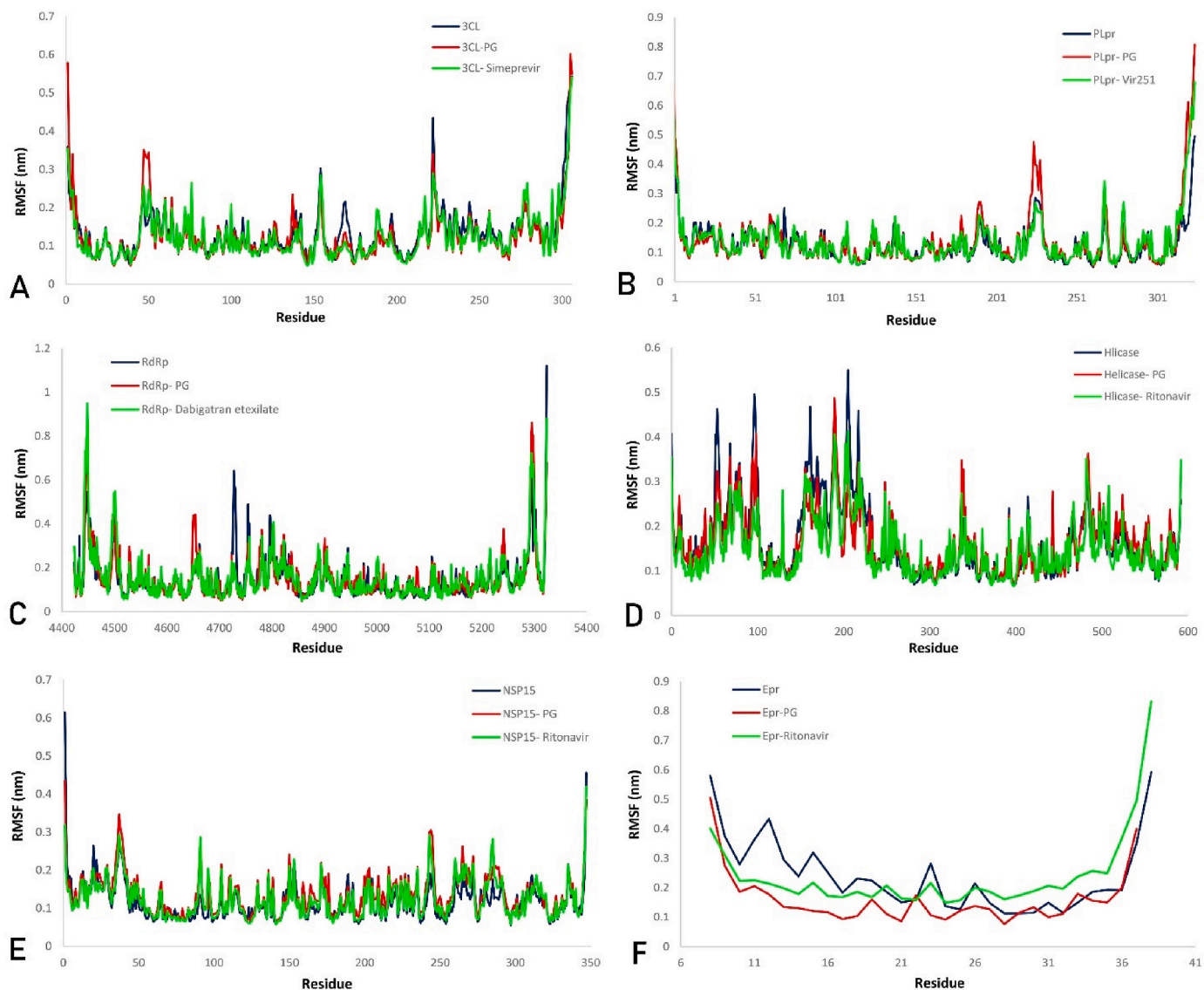


Fig. 4. The plots of RMSF for all interactions. (A) 3CLpro's complexes (B) PLpro's complexes (C) RdRp's complexes (D) helicase's complexes (E) NSP15's complexes (F) E protein's complexes.

The average LJ potential of helicase in in complex with PG and Ritonavir were -119.608 and -163.16 kJ/mol, respectively. Meanwhile, the lower LJ potential value of PG than Ritonavir indicated its relatively constant fluctuation during the 100 ns, which is presented in Fig. 2D. Therefore, PG can be considered as a qualified potent inhibitor for helicase.

The average LJ potential of PG and Ritonavir in interaction with NSP15 were -88.70 and -65.23 kJ/mol, respectively. According to Fig. 2E, although both ligands contained high fluctuations throughout 100 ns; however, Ritonavir exhibited a higher and more severe fluctuation than PG. Therefore, in contrast to its superior interaction with NSP15, PG may be incapable of performing the explicit targeting of this protein.

The average LJ potentials of E protein in interaction with PG and Ritonavir were -213.33 and -192.092 kJ/mol, respectively. In contrast to Ritonavir, PG demonstrated a minor and constant fluctuation throughout the simulation, which is displayed in Fig. 2F. As a result, PG proved its ability to target the E protein through the formation of an utterly stable interaction.

3.2.2. Root mean square deviation (RMSD)

In this section, we calculated the Root-Mean-Square Deviation active site (RMSD_{as}) of proteins active site to investigate the change conformation and stability of the active site residues in interaction with PG and inhibitory ligands. It should be noted that the low value of RMSD represents the high stability of a complex.

In conformity to Fig. 3A, the connection of PG to 3CLpro displayed a relatively similar fluctuation to that of free 3CLpro and 3CLpro-Simeprevir complex, which proves the existence of a stable interaction with this target.

Based on Fig. 3B, the RMSD_{as} of PLpro in interaction with PG declined. However, in comparison with the complex of PLpro and Vir251, the performance of PG was relatively weaker than the inhibitory ligand. Nevertheless, PG is still capable of forming a stable interaction with PLpro due to the average RMSD_{as} of free PLpro and its complex with PG, which were 0.21 and 0.2 nm, respectively. According to previous Data, the achievement of an RMSD in the range of 0.2–0.3 nm indicates the stability of an interaction.

Considering Fig. 3C, the connection of PG to RdRp caused a decrease in the RMSD_{as} of this target and displayed a superior performance than that of Dabigatran etexilate, which is indicative of a stable and robust

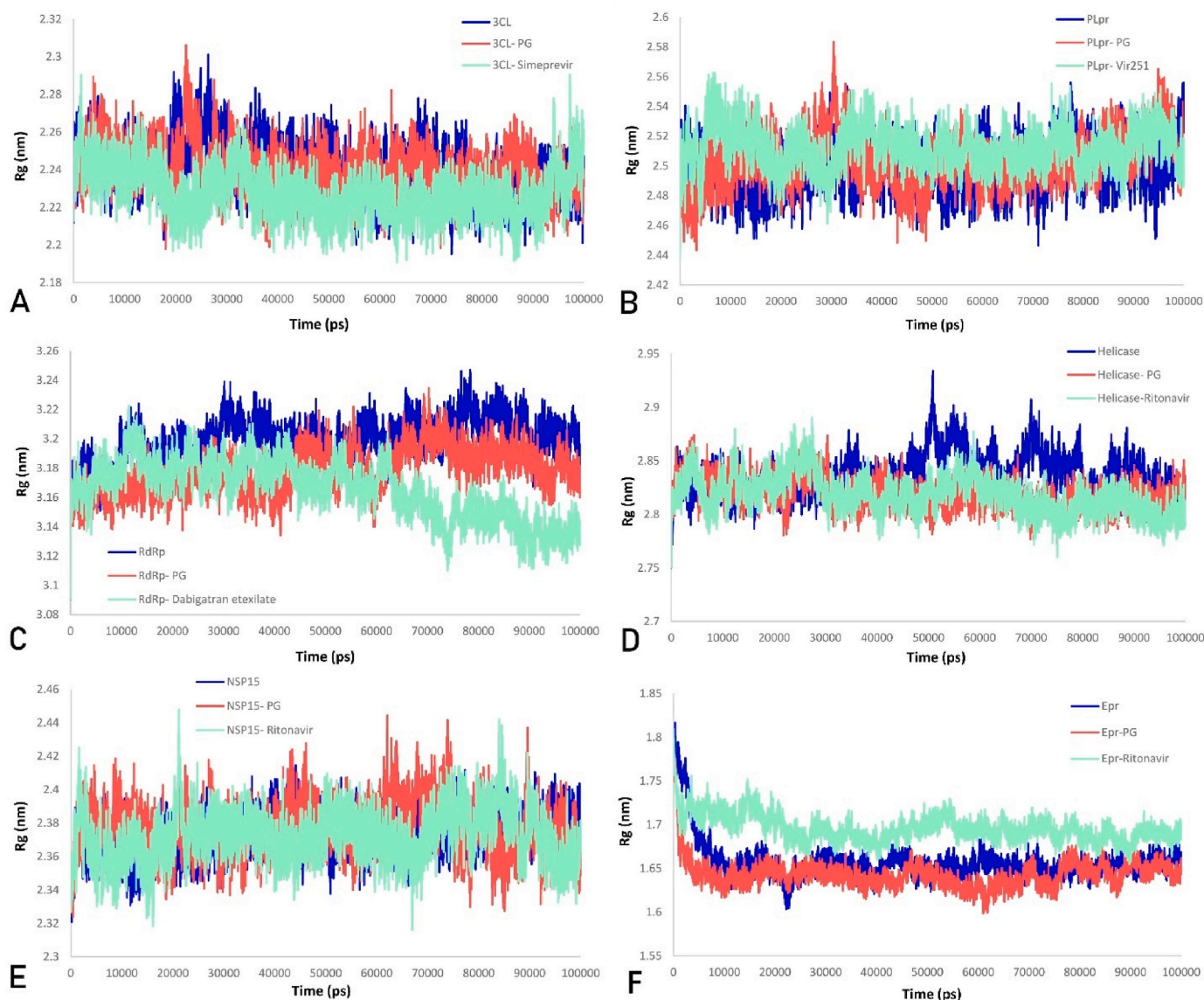


Fig. 5. The plots of Rg for all interactions. (A) 3CLpro's complexes (B) PLpro's complexes (C) RdRp's complexes (D) helicase's complexes (E) NSP15's complexes (F) E protein's complexes.

interaction with RdRp.

In conformity to Fig. 3D, the RMSDAs of helicase in complex with PG and Ritonavir was increased, while a slight increase in the RMSDAs of PG in complex to this protein was observed when compared to the results of Ritonavir. The occurrence of these raises may be due to the competition of water molecules with ligands throughout the active sites of protein [56]. Moreover, the existence of some loops and turns throughout the active site of helicase resulted in causing the highest rate of fluctuations in interacting with ligands. Therefore, the ability of PG to create a sufficient and stable interaction with helicase was approved.

According to Fig. 3E, the average RMSDAs of NSP15 and its complex with PG and Ritonavir were 0.19 nm, 0.21 nm, and 0.2 nm, respectively. Consequently, it is assumed that PG and the inhibitor ligand displayed a relatively similar behavior upon interaction with NSP15 and therefore, PG could be considered as a suitable inhibitor for this target.

Based on Fig. 3F, the average RMSDAs of E protein and its complex with PG and Ritonavir were 0.3 nm, 0.48 nm, and 0.54 nm, respectively. The high values of RMSDAs in both cases of PG and inhibitory ligand was caused by their interaction with ion-channels C-terminal that are attached to the free carboxyl end of this protein. Moreover, another

reason for this increase may be the competition of ligands with water molecules throughout the binding site. Therefore, PG achieved a better RMSDAs value than Ritonavir, and its LJ potential in interaction with E protein verified its ability in forming a more stable and solid interaction.

3.2.3. Root mean square fluctuation (RMSF)

The root mean square fluctuation (RMSF) analysis determines the fluctuation of residues throughout a simulation. In contrast to the regular secondary structures, which contain less fluctuation and mobility, the irregular secondary structures exhibit more fluctuation and mobility. The average RMSF of all systems is demonstrate in Table 2 and the plots of RMSF for every complex is depicted in Fig. 4. In the case of PG interaction with 3CLpro, helicase and E protein caused a decrease in the RMSF of proteins and active site. In addition, this ligand displayed a better performance in interaction with these proteins, while the application of PG caused a further reduction in the RMSF value when compared to the results of inhibitor ligands. The connection of PG to PLpro, RdRp, and NSP15, induced a slight increase in the RMSF value due to the irregular secondary structures, such as coil and turn in the active site of these proteins exist; therefore, both PG and inhibitor

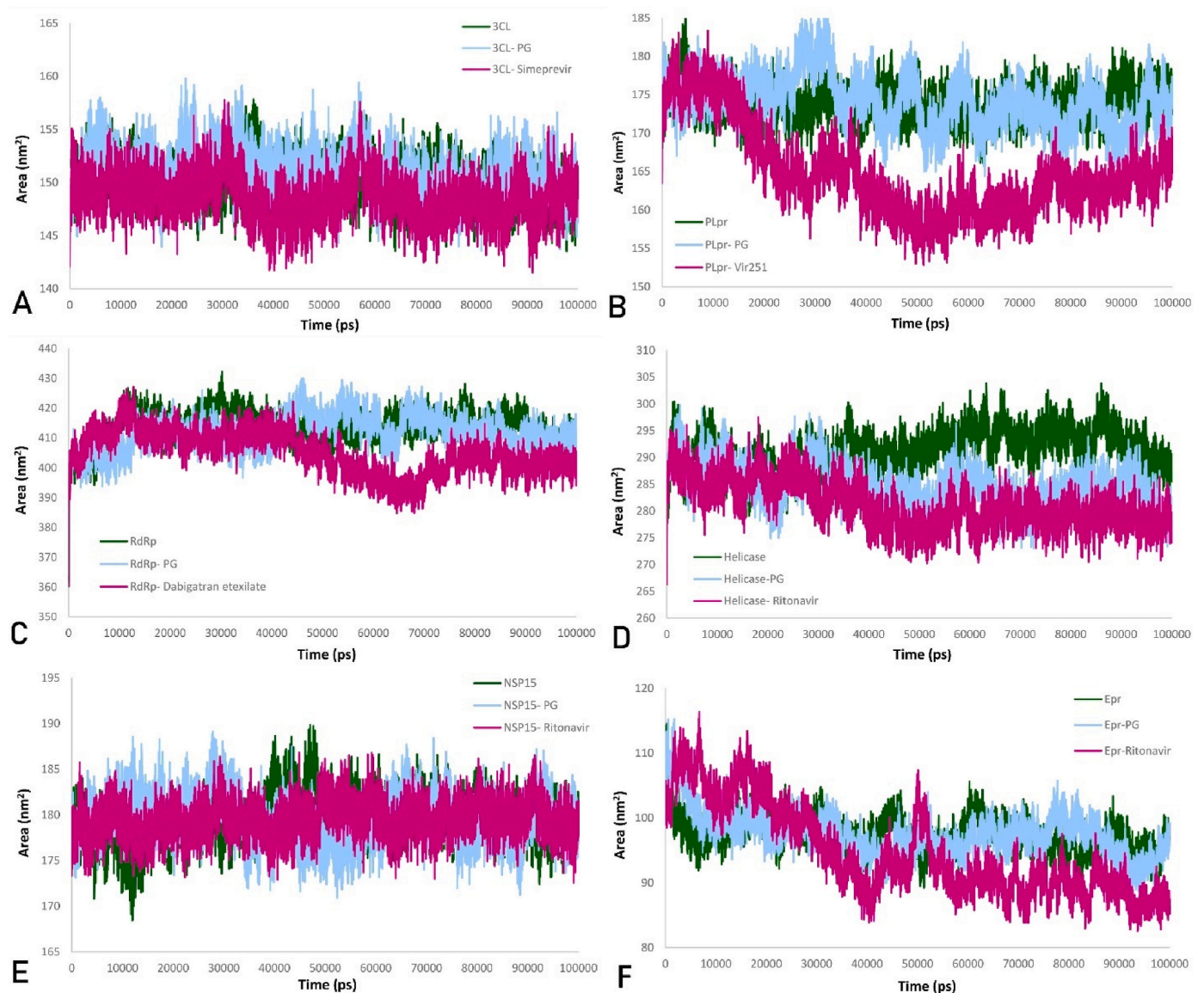


Fig. 6. The plots of SASA for all interactions. (A) 3CLpro's complexes (B) PLpro's complexes (C) RdRp's complexes (D) helicase's complexes (E) NSP15's complexes (F) E protein's complexes.

Table 3
DSSP analyses.

Complexes	Structure (α -helix + β -sheet + β -bridge + turn)
3CLpro	0.64
3CLpro-PG	0.65
3CLpro- Simeprevir	0.63
PLpro	0.68
PLpro-PG	0.65
PLpro-Vir251	0.68
RdRp	0.65
RdRp-PG	0.65
RdRp- Dabigatran etexilate	0.65
Helicase	0.58
Helicase-PG	0.59
Helicase-Ritonavir	0.58
NSP15	0.61
NSP15-PG	0.62
NSP15-Ritonavir	0.62
E protein	0.85
E protein-PG	0.84
E protein-Ritonavir	0.82

ligands displayed a relatively higher value of RMSF than the free proteins. However, the structures of proteins were not disrupted by these increases, which enabled PG to create stable and appropriate interactions with all of the targets.

3.2.4. Radius of gyration (R_g)

R_g is evaluated the protein compactness and the change conformation of protein after binding ligand. A higher value of R_g refers to the looser fold of protein structure, whereas a lower value relates to a stiffer and more compact protein structure. Fig. 5 portrays the radius of gyration for all the systems, and Table 2 depicts their average value of R_g throughout the 100 ns. Based on the presented data, the connection of PG to targets did not cause any abnormal change conformation or compactness of targets, while PG displayed a relatively similar behavior to the inhibitor ligands.

3.2.5. Solvent Accessible Surface Area (SASA)

The analyzing method of solvent-accessible surface area (SASA) is used to examine the compactness and accessible area of the receptor in regard to the solvent. Apparently, the presences of hydrophobic amino

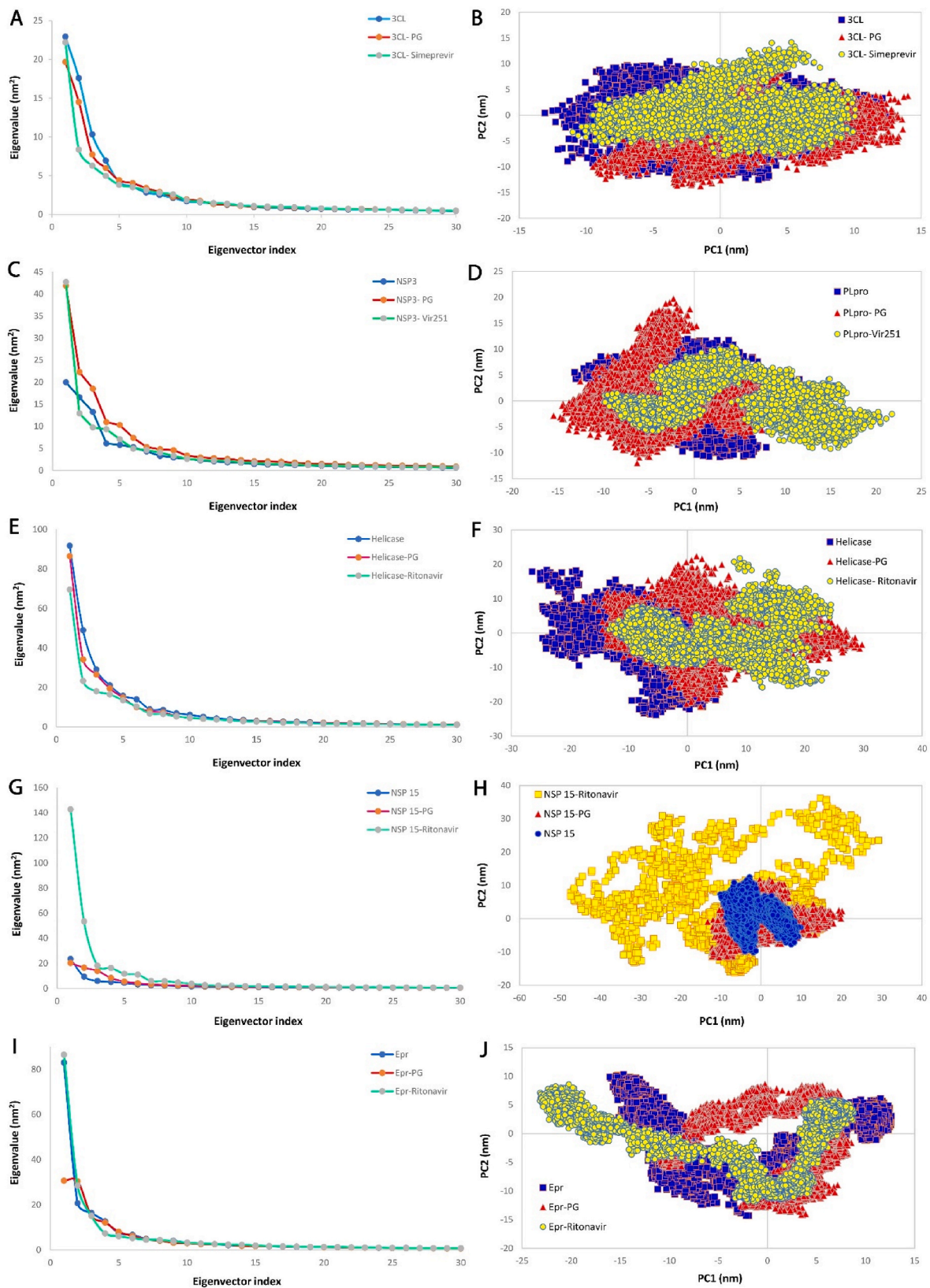


Fig. 7. The plots of PCA analyses. (A) The plot of first 30 eigenvectors index against eigenvalues show PCA analysis 3CLpro and its complexes (B) The plot demonstrates the 2D projection of PC1 and PC2 for 3CLpro and its complexes (C) The plot of first 30 eigenvectors index against eigenvalues show PCA analysis PLpro and its complexes (D) The plot demonstrates the 2D projection of PC1 and PC2 for PLpro and its complexes (E) The plot of first 30 eigenvectors index against eigenvalues show PCA analysis helicase and its complexes (F) The plot demonstrates the 2D projection of PC1 and PC2 for helicase and its complexes (G) The plot of first 30 eigenvectors index against eigenvalues show PCA analysis NSP15 and its complexes (H) The plot demonstrates the 2D projection of PC1 and PC2 for NSP15 and its complexes (I) The plot of first 30 eigenvectors index against eigenvalues show PCA analysis E protein and its complexes (J) The plot demonstrates the 2D projection of PC1 and PC2 for E protein and its complexes.

Table 4
The interaction results of all complexes in the last snapshot of MD simulation.

Complex's name	Interaction	Distance	E (kcal/mol)
3CLpro-PG	GLU 166 (A) H-donor	2.72	-5.2
	ARG 188 (A) H-donor	2.70	-2.6
	THR 190 (A) H-donor	2.84	-2.0
	ASP 48 (A) H-donor	2.95	-0.8
	ASN 142 (A) pi-H	3.67	-0.5
3CLpro-Simeprevir	GLU 166 (A) H-donor	2.54	-10.5
	GLU 166 (A) H-donor	3.25	-0.5
	GLU 166 (A) Ionic	2.54	-8.4
	GLN 189 (A) H-acceptor	2.76	-3.2
PLpro-PG	ALA 246 (A) H-donor	2.83	-1.3
	LEU 162 (A) H-donor	2.76	-1.6
	TYR 268 (A) pi-pi	3.95	-0.0
PLpro-Vir251	GLN 269 (A) H-donor	3.28	-0.7
	GLY 163 (A) H-donor	2.68	-4.8
	GLY 163 (A) H-acceptor	3.03	-3.6
	GLY 271 (A) H-donor	2.73	-4.4
RdRp-PG	TYR 264 (A) H-acceptor	2.68	-3.5
	SER 549 (A) H-donor	2.99	-0.7
	ASP 760 (A) H-donor	3.10	-2.8
	THR 687 (A) H-donor	2.70	-2.1
	LYS 551 (A) H-donor	2.85	-2.3
	TYR 619 (A) H-donor	2.50	-3.7
	LYS 621 (A) H-acceptor	2.75	-8.4
	2: ARG 555 (A) H-acceptor	2.86	-4.0
	2: LYS 545 (A) pi-H	3.98	-0.9
RdRp-Dabigatran	ASP 761 (A) H-donor	2.62	-8.2
	2: ASP 618 (A) 1: H-donor	2.84	-4.2
	(A) 1: Ionic	2.84	-5.7
	ASP 761 (A) Ionic	2.62	-7.5
	ASP 623 (A) pi-H	3.69	-1.0
NSP13-PG	2: GLU 375 (A) H-donor	2.48	-2.6
		2.61	-6.1
NSP13-Ritonavir	GLU 319 (A) H-donor	2.53	-4.7
	4: GLU 375 (A) 2: H-donor	3.04	-2.9
		2.66	-11.9
	2: Ionic	3.04	-4.2
		2.66	-7.2
NSP15-PG	HIS 290 (A) H-donor	3.77	-0.7
	LYS 320 (A) H-acceptor	2.87	-4.1
	2: GLU 340 (A) 2: H-donor	2.68	-2.1
		2.70	-5.7
NSP15-Ritonavir	2: TYR 343 (A) 1: H-acceptor	2.78	-2.5
	1: pi-pi	3.91	-0.0
	TRP 333 (A) pi-pi	3.67	-0.0
	ASP 240 (A) H-donor	2.53	-8.2
	ASP 240 (A) Ionic	2.53	-8.6
Epr-PG	TRP 333 (A) H-pi	4.70	-0.6
	THR 35 (E) H-donor	3.21	-0.6
Epr-Ritonavir	ALA 32 (A) pi-H	3.81	-0.6

acids cause an increase in the SASA value [57]. In comparison to the inhibitor ligands, Table 2 exhibits a hardly increased in the SASA values of PG in interactions with 3CLpro, PLpro, RdRp, NSP15, and E protein due to the larger number of hydrophobic residues around the PG throughout these interactions. The SASA value of PG in interaction with helicase was a little higher than Ritonavir due to the wider exposure of PG to the solvents, which prevented the inducement of any abnormal changes in the structure (Fig. 6). As confirmed by the data of Rg, the observance of a slight change indicated the binding of PG to the targets and proved its ability to act as a qualified inhibitor for these targets. On the other hand, PG in interaction with RdRp and helicase indicated a lower value of SASA than free protein, thus this ligand can create a more stable interaction with these two targets.

3.2.6. Dictionary of secondary structure of proteins (DSSP)

The results of DSSP analysis can identify the secondary structure of a protein and portray the inducement of any change conformation by binding ligand. Table 3 presents the data of DSSP throughout the 100 ns

and accordingly, the binding of PG to each of the targets did not cause any significant changes in the secondary structure.

3.2.7. The essential dynamics (ED)

Principal component analysis (PCA) or essential dynamics (ED) is used to characterize any motions or change conformation in the structure of proteins in complex with ligands. Since the first few eigenvectors represent the most protein movement, we picked the first 30 eigenvectors to estimate the protein's motion, which is plotted in Fig. 7. The 2D projection plot of PCA portrays the overall dynamics of proteins in complex with ligands. Considering how the first two PCs provide the most important information about the movement of protein, the first two eigenvectors were selected and plotted against each other for every complex.

Fig. 7B presents the 2D projection plot of 3CLpro in complex with PG and Simeprevir. The motions of protein faced a decreased in the course of 3CLpro interaction with PG (Fig. 7A), while the plots of 3CLpro-PG complex were observed to occupy less space than the solitary case of 3CLpro. Although the functionality of PG was not as strong as Simeprevir, which is in contrast to the inhibitory ligand, but it was capable of inhibiting 3CLpro and creating a stable interaction with this target.

The 2D projection plot of PLpro in complex to PG and Vir251 is displayed in Fig. 7D. While the effects of both PG and inhibitory ligand caused an increase in the binding motion (Fig. 7C), yet the interaction between PLpro with PG faced a higher increase. This complex also occupied a more prominent space than the solitary cases of Vir251 and PLpro. Therefore, the inhibitory function of PG may be less significant than that of Vir251.

In conformity to Fig. 7F, the connection of PG to helicase led to the occupancy of relatively similar space to that of helicase alone, while the helicase-PG complex took more space than the helicase-Ritonavir complex. The interaction of PG with helicase resulted in decreasing the protein motion and indicated its ability to form a stable interaction with this protein (Fig. 7E). Accordingly, PG can also function against helicase in the role of an adequate inhibitor.

In conformity to Fig. 7H, the occupied space of NSP15-PG complex was less than the NSP15-Ritonavir complex, which expresses the superior potential of PG than the inhibitory ligand in inhibiting NSP15 and creating a more stable interaction. Next to a better performance, the interaction of PG with this target caused a higher decrease in the protein motion than Ritonavir, which is a stronger performance than Ritonavir (Fig. 7G). However, it is possible that this protein was not the main target of PG, since the LJ potential of this target in complex with PG and Ritonavir confirmed this assumption as well.

Based on Fig. 7J, the E protein-PG complex occupied less space than complex of solitary the E protein and E protein-Ritonavir complex. Moreover, Fig. 7 I displays the interaction of PG with E protein, which caused a decrease in the motion of this target and in contrast to the inhibitory ligand, exhibited a remarkably superior performance. Therefore, it can be assumed that PG is capable of creating a solid and stable interaction with E protein and function as a potential and practical inhibitor of this protein.

4. Discussion

The spreading of COVID-19 pandemic since 2019 has led to the death of millions of people worldwide and unfortunately, scientific approaches were incapable of finding any reliable way to suppress this virus completely. Several types of research disclosed the antiviral, anti-inflammatory, antimicrobial, antinociceptive, antioxidant, and anti-tumor properties of *Pistacia* sp., which can also cause potential impacts on gastrointestinal disorders. In this research, we investigated the effects of active ingredients, obtained from five species of *Pistacia*, on the most crucial protein targets of SARS-COV-2 including 3CLpro, PLpro, RdRp, helicase, NSP15, and E protein. According to the results of molecular docking, PG was the most potent and robust active ingredient of *Pistacia*

lentiscus in interaction with all of the selected targets. The binding energies of docking process indicated that initially, PG displayed a high binding affinity with helicase (−10.76 kcal/mol) and RdRp (−10.19 kcal/mol) and created the solid and firm interaction through the production of ionic and hydrogen bonds. In the following, this ingredient exhibited a very suitable tendency to interact with E protein (−9.51 kcal/mol) and 3CLpro (−9.47 kcal/mol) while forming a vigorous interaction with these two targets by developing hydrogen bonds during the docking process and simulation. Thirdly, the acceptable interactions of PG with NSP15 (−8.65 kcal/mol) and PLpro (−8.06 kcal/mol) were confirmed through the observance of hydrogen, ionic, and pi-pi bonds. Meanwhile, PG was ideally located in the active site of selected targets throughout every interaction. In addition, the last snapshot from the 100 ns simulation (Table 4) verified its ability to create an utterly stable and solid interaction with the proteins in the course of the simulation without displaying any alterations in its position. In conformity to the LJ potential data, PG was capable of forming steadily interactions with 3CLpro, RdRp, E protein, and helicase, while exhibiting a suitable and superior performance when compared to the inhibitory ligand of these four targets. According to the outcomes of RMSDAs, the RdRp-PG complex and 3CLpro-PG complex contained a lower RMSDAs than the free proteins and complexes of inhibitory ligands. Consequently, the higher stability of PG's interactions with RdRp and 3CLpro, as well as its satisfactory performance in complex with these two targets especially RdRp, can be confirmed. The results of Rg, SASA, and RMSF approved the superior and more adequate performance of PG upon interacting with RdRp, helicase, E protein, and 3CLpro which was also able to thoroughly inhibit these targets and form stable interactions in contrast to the other targets. As the final step, PCA analysis displayed the induced reduction in the motion of E protein, 3CLpro, and helicase and particularly E protein due to their interaction with PG, which portrayed the potential of our selected ligand (PG) as a capable inhibitor for E protein, 3CLpro, and helicase.

5. Conclusion

In summary, our study revealed significant data on the inhibitory activity of PG, which is the most effective ingredient of *Pistacia lentiscus*, in interactions with the most significant protein targets on SARS-COV-2. The results of molecular docking and MD simulations confirmed the strong inhibitory effect of PG on RdRp, helicases, 3CLpro and E protein, forming a stable and strong interaction with these targets. Therefore, this paper proposes the possibility of preventing the process of replication and transcription of SARS-COV-2 through the inhibitory action of PG on RdRp, helicase, 3CLpro and E protein. We hope that our research will drive the development of an original approach to the treatment of COVID-19.

Funding

This work was supported financially by the Research Council of Mashhad University of Medical Sciences.

Authors' contributions

F. S., Z. A.T., and J. C. designed the research study; Z. A.T. and F. S. conducted an investigation and amassed the data; Z. A.T., J. C., and F. S. analyzed the data; F. S. and Z. A.T. wrote the initial draft of the manuscript. M. R. S. and J. C. revised the manuscript; All authors debated the results and contributed to the final manuscript.

Declaration of interest

Declarations of interest: none.

Acknowledgements

The department of Medicinal Chemistry, School of Pharmacy, Mashhad University of Medical Sciences, is gratefully acknowledged for supporting this project and providing facilities.

Appendix A. Supplementary data

Supplementary data to this article can be found online at <https://doi.org/10.1016/j.mcp.2022.101847>.

Abbreviations

SARS-CoV-2	severe acute respiratory syndrome-coronavirus-2
COVID-19	coronavirus disease 2019
<i>Pistacia</i> sp.	<i>Pistacia species</i>
3CLpr	3-chymotrypsin-like protease
PLpro	Papain-like protease
RdRp	RNA dependent RNA polymerase
NSP15	Nonstructural protein-15 (endoRNase)
E protein	Envelope protein
PG	1,2,3,4,6-pentagalloyl glucose
MD	Molecular dynamic
RMSDAs	Root mean square deviations of active site
RMSF	Root mean square fluctuations
Rg	Radius of gyration
PCA	Principal components analysis
ED	The essential dynamics
SASA	Solvent Accessible Surface Area
DSSP	Dictionary of secondary structure of proteins
LJ	Lennard-Jones potential

References

- [1] F. Mahjoub, K.A. Rezayat, M. Yousefi, M. Mohebbi, R. Salari, *Pistacia atlantica* Desf. A review of its traditional uses, phytochemicals and pharmacology, *Journal of medicine and life* 11 (3) (2018) 180–186.
- [2] M. Bozorgi, Z. Memariani, M. Mobli, M.H. Salehi Surmaghi, M.R. Shams-Ardekani, R. Rahimi, Five *Pistacia* species (*P. vera*, *P. atlantica*, *P. terebinthus*, *P. khinjuk*, and *P. lentiscus*): a review of their traditional uses, phytochemistry, and pharmacology, *Sci. World J.* (2013), 2013.
- [3] M. Kashaninejad, A. Mortazavi, A. Safekordi, L. Tabil, Some physical properties of *Pistachio* (*Pistacia vera* L.) nut and its kernel, *J. Food Eng.* 72 (1) (2006) 30–38.
- [4] B. Özçelik, M. Aslan, I. Orhan, T. Karaoglu, Antibacterial, antifungal, and antiviral activities of the lipophilic extracts of *Pistacia vera*, *Microbiol. Res.* 160 (2) (2005) 159–164.
- [5] E.M. Giner-Larza, S. Máñez, R.M. Giner-Pons, M.C. Recio, J.-L. Ríos, On the anti-inflammatory and anti-phospholipase A2 activity of extracts from lanostane-rich species, *J. Ethnopharmacol.* 73 (1–2) (2000) 61–69.
- [6] O. Tzakou, I. Bazos, A. Yannitsaros, Volatile metabolites of *pistacia atlantica* desf. From Greece, *Flavour Fragrance J.* 22 (5) (2007) 358–362.
- [7] H. Hosseinzadeh, E. Behravan, M.M. Soleimani, Antinociceptive and anti-inflammatory effects of *pistacia vera* LeafExtract in mice, *Iran. J. Pharm. Res. (IJPR)*: 10 (4) (2011) 821.
- [8] H. Benamar, W. Rached, A. Derdour, A. Marouf, Screening of Algerian medicinal plants for acetylcholinesterase inhibitory activity, *J. Biol. Sci.* 10 (1) (2010) 1–9.
- [9] M. Ramezani, M. Khaje-Karamoddi, V. Karimi-Fard, Chemical Composition and anti-*helicobacter pylori* activity of the essential oil of *pistacia vera*, *Pharmaceut. Biol.* 42 (7) (2004) 488–490.
- [10] C. Gardeli, P. Vassiliki, M. Athanasios, T. Kibouris, M. Komaitis, Essential oil composition of *Pistacia lentiscus* L. and *Myrtus communis* L.: evaluation of antioxidant capacity of methanolic extracts, *Food Chem.* 107 (3) (2008) 1120–1130.
- [11] W. Bhouri, S. Derbel, I. Skandrani, J. Boubaker, I. Bouhlel, M.B. Sghaier, et al., Study of genotoxic, antigenotoxic and antioxidant activities of the digallic acid isolated from *Pistacia lentiscus* fruits, *Toxicol. Vitro* 24 (2) (2010) 509–515.
- [12] A. Abdelwahed, I. Bouhlel, I. Skandrani, K. Valenti, M. Kadri, P. Guiraud, et al., Study of antimutagenic and antioxidant activities of Gallic acid and 1, 2, 3, 4, 6-pentagalloylglucose from *Pistacia lentiscus*: confirmation by microarray expression profiling, *Chem. Biol. Interact.* 165 (1) (2007) 1–13.
- [13] K. Balan, J. Prince, Z. Han, K. Dimas, M. Cladaras, J. Wyche, et al., Antiproliferative activity and induction of apoptosis in human colon cancer cells treated in vitro with constituents of a product derived from *Pistacia lentiscus* L. var. *chia*, *Phytomedicine* 14 (4) (2007) 263–272.
- [14] S. Magkouta, G.T. Stathopoulos, I. Psallidas, A. Papapetropoulos, F.N. Kolisis, C. Roussos, et al., Protective effects of mastic oil from *Pistacia lentiscus* variation

- chia against experimental growth of lewis lung carcinoma, *Nutr. Cancer* 61 (5) (2009) 640–648.
- [15] C. Giaginis, S. Theocharis, Current evidence on the anticancer potential of Chios mastic gum, *Nutr. Cancer* 63 (8) (2011) 1174–1184.
- [16] A. Peksel, I. Arisan-Atac, R. Yanardag, Evaluation of antioxidant and antiacetylcholinesterase activities of the extracts of *Pistacia atlantica* Desf. Leaves, *J. Food Biochem.* 34 (3) (2010) 451–476.
- [17] I. Hamdan, F. Afifi, Studies on the in vitro and in vivo hypoglycemic activities of some medicinal plants used in treatment of diabetes in Jordanian traditional medicine, *J. Ethnopharmacol.* 93 (1) (2004) 117–121.
- [18] V. Kasabri, F.U. Afifi, I. Hamdan, In vitro and in vivo acute antihyperglycemic effects of five selected indigenous plants from Jordan used in traditional medicine, *J. Ethnopharmacol.* 133 (2) (2011) 888–896.
- [19] A. Triantafyllou, N. Chaviaras, T.N. Sergentanis, E. Protopapa, J. Tsaknis, Chios mastic gum modulates serum biochemical parameters in a human population, *J. Ethnopharmacol.* 111 (1) (2007) 43–49.
- [20] S. Nazifi, M. Saeb, M. Sepehrimaneh, S. Poorgonabadi, The effects of wild pistachio oil on serum leptin, thyroid hormones, and lipid profile in female rats with experimental hypothyroidism, *Comp. Clin. Pathol.* 21 (5) (2012) 851–857.
- [21] K.A. Marinou, K. Georgopoulou, G. Agrogiannis, T. Karatzas, D. Iliopoulos, A. Papalois, et al., Differential effect of *Pistacia vera* extracts on experimental atherosclerosis in the rabbit animal model: an experimental study, *Lipids Health Dis.* 9 (1) (2010) 1–9.
- [22] T. Bakirel, S. Şener, U. Bakirel, O. Keleş, G. Şennazlı, A. Gürel, The investigation of the effects of *Pistacia terebinthus* L. upon experimentally induced hypercholesterolemia and atherosclerosis in rabbits, *Turk. J. Vet. Anim. Sci.* 27 (6) (2003) 1283–1292.
- [23] N. Tanideh, S. Masoumi, M. Hosseinzadeh, A.R. Safarpour, H. Erjaee, O. Koohi-Hosseinabadi, et al., Healing effect of *pistacia atlantica* fruit oil extract in acetic Acid-induced colitis in rats, *Iran. J. Med. Sci.* 39 (6) (2014) 522–528.
- [24] E. Milia, S.M. Bullitta, G. Mastandrea, B. Szotáková, A. Schoubben, L. Langhansová, et al., Leaves and fruits preparations of *pistacia lentiscus* L.: a review on the ethnopharmacological uses and implications in inflammation and infection, *Antibiotics* 10 (4) (2021) 425.
- [25] M.C. Nirumand, M. Hajjalayani, R. Rahimi, M.H. Farzaei, S. Zingue, S.M. Nabavi, et al., Dietary plants for the prevention and management of kidney stones: preclinical and clinical evidence and molecular mechanisms, *Int. J. Mol. Sci.* 19 (3) (2018) 765.
- [26] R.H. Chen, L.J. Yang, S. Hamdoun, S.K. Chung, CW-k Lam, K.X. Zhang, et al., 1, 2, 3, 4, 6-Pentagalloyl glucose, a RBD-ACE2 binding inhibitor to prevent SARS-CoV-2 infection, *Front. Pharmacol.* 12 (2021), 634176.
- [27] Y.C. Guillaume, C. André, Immobilization of the SARS-CoV-2-receptor binding domain onto methacrylate-based monoliths for nano LC at 30 nL min⁻¹ and application for research of its ligands, *Anal. Methods* 14 (2) (2022) 156–164.
- [28] R. Arya, S. Kumari, B. Pandey, H. Mistry, S.C. Bihani, A. Das, et al., Structural insights into SARS-CoV-2 proteins, *J. Mol. Biol.* 433 (2) (2021), 166725.
- [29] Z. Jin, X. Du, Y. Xu, Y. Deng, M. Liu, Y. Zhao, et al., Structure of M pro from SARS-CoV-2 and discovery of its inhibitors, *Nature* 582 (7811) (2020) 289–293.
- [30] La Alanagreh, F. Alzoughool, M. Atoum, The human coronavirus disease COVID-19: its origin, characteristics, and insights into potential drugs and its mechanisms, *Pathogens* 9 (5) (2020) 331.
- [31] F.K. Yoshimoto, The proteins of severe acute respiratory syndrome coronavirus-2 (SARS CoV-2 or n-COV19), the cause of COVID-19, *Protein J.* 39 (2020) 198–216.
- [32] S. Skariyachan, D. Gopal, A.G. Muddebhalkar, A. Uttarkar, V. Niranjan, Structural insights on the interaction potential of natural leads against major protein targets of SARS-CoV-2: molecular modelling, docking and dynamic simulation studies, *Comput. Biol. Med.* 132 (2021), 104325.
- [33] M. Behbahani, In silico Design of novel Multi-epitope recombinant Vaccine based on Coronavirus surface glycoprotein, *bioRxiv* (2020).
- [34] M. Kim, M. Cho, J.-H. Lee, H. Kim, H.S. Son, Analysis of coronaviral spike proteins and virus–host interactions, *Korean J. Public Health* 56 (1) (2019) 25–32.
- [35] D. Schoeman, B.C. Fielding, Coronavirus envelope protein: current knowledge, *Virology* 16 (1) (2019) 1–22.
- [36] P. Venkatagopalan, S.M. Daskalova, L.A. Lopez, K.A. Dolezal, B.G. Hogue, Coronavirus envelope (E) protein remains at the site of assembly, *Virology* 478 (2015) 75–85.
- [37] J.L. Nieto-Torres, M.L. DeDiego, E. Álvarez, J.M. Jiménez-Guardeño, J.A. Regla-Nava, M. Llorente, et al., Subcellular location and topology of severe acute respiratory syndrome coronavirus envelope protein, *Virology* 415 (2) (2011) 69–82.
- [38] N. Tripathi, B. Goel, N. Bhardwaj, B. Sahu, H. Kumar, S.K. Jain, Virtual screening and molecular simulation study of natural products database for lead identification of novel coronavirus main protease inhibitors, *J. Biomol. Struct. Dyn.* (2020) 1–13.
- [39] C.B. Mishra, P. Pandey, R.D. Sharma, M.Z. Malik, R.K. Mongre, A.M. Lynn, et al., Identifying the natural polyphenol catechin as a multi-targeted agent against SARS-CoV-2 for the plausible therapy of COVID-19: an integrated computational approach, *Briefings Bioinf.* 22 (2) (2021) 1346–1360.
- [40] Z. Jin, X. Du, Y. Xu, Y. Deng, M. Liu, Y. Zhao, et al., Structure of Mpro from SARS-CoV-2 and discovery of its inhibitors, *Nature* 582 (7811) (2020) 289–293.
- [41] W. Rut, Z. Lv, M. Zmudzinski, S. Patchett, D. Nayak, S.J. Snipas, et al., Activity profiling and crystal structures of inhibitor-bound SARS-CoV-2 papain-like protease: a framework for anti-COVID-19 drug design, *Sci. Adv.* 6 (42) (2020), eabd4596.
- [42] Y. Gao, L. Yan, Y. Huang, F. Liu, Y. Zhao, L. Cao, et al., Structure of the RNA-dependent RNA polymerase from COVID-19 virus, *Science* 368 (6492) (2020) 779–782.
- [43] V.S. Mandala, M.J. McKay, A.A. Shcherbakov, A.J. Dregni, A. Kolocouris, M. Hong, Structure and drug binding of the SARS-CoV-2 envelope protein transmembrane domain in lipid bilayers, *Nat. Struct. Mol. Biol.* 27 (12) (2020) 1202–1208.
- [44] J.A. Newman, A. Douangamath, S. Yazdani, Y. Yosaatmadja, A. Aimon, J. Brandão-Neto, et al., Structure, mechanism and crystallographic fragment screening of the SARS-CoV-2 NSP13 helicase, *Nat. Commun.* 12 (1) (2021) 1–11.
- [45] Y. Kim, J. Wower, N. Maltseva, C. Chang, R. Jedrzejczak, M. Wilamowski, et al., Tipiracil binds to uridine site and inhibits Nsp15 endoribonuclease NendoU from SARS-CoV-2, *Commun. Biol.* 4 (1) (2021) 1–11.
- [46] K.M. Merz Jr., D. Ringe, C.H. Reynolds, *Drug Design: Structure-And Ligand-Based Approaches*, Cambridge University Press, 2010.
- [47] A.A. Alrasheid, M.Y. Babiker, T.A. Awad, Evaluation of certain medicinal plants compounds as new potential inhibitors of novel corona virus (COVID-19) using molecular docking analysis, *Silico Pharmacol.* 9 (1) (2021) 1–7.
- [48] P. Labute, The generalized Born/volume integral implicit solvent model: estimation of the free energy of hydration using London dispersion instead of atomic surface area, *J. Comput. Chem.* 29 (10) (2008) 1693–1698.
- [49] C. Kutzner, S. Páll, M. Fechner, A. Esztermann, B.L. de Groot, H. Grubmüller, More bang for your buck: improved use of GPU nodes for GROMACS 2018, *J. Comput. Chem.* 40 (27) (2019) 2418–2431.
- [50] A. Croitoru, S.-J. Park, A. Kumar, J. Lee, W. Im, A.D. MacKerell Jr., et al., Additive CHARMM36 force field for nonstandard amino acids, *J. Chem. Theor. Comput.* 17 (6) (2021) 3554–3570.
- [51] P. Rosales-Pelaez, I. Sanchez-Burgos, C. Valeriani, C. Vega, E. Sanz, Seeding approach to nucleation in the NVT ensemble: the case of bubble cavitation in overstretched Lennard Jones fluids, *Phys. Rev.* 101 (2) (2020), 022611.
- [52] S. Vardhan, S.K. Sahoo, In silico ADMET and molecular docking study on searching potential inhibitors from limonoids and triterpenoids for COVID-19, *Comput. Biol. Med.* 124 (2020), 103936.
- [53] S.A. Amin, S. Banerjee, K. Ghosh, S. Gayen, T. Jha, Protease targeted COVID-19 drug discovery and its challenges: insight into viral main protease (Mpro) and papain-like protease (PLpro) inhibitors, *Bioorg. Med. Chem.* 29 (2021), 115860.
- [54] R. Vivek-Ananth, S. Krishnaswamy, A. Samal, Potential phytochemical inhibitors of SARS-CoV-2 helicase Nsp13: a molecular docking and dynamic simulation study, *Mol. Divers.* 26 (1) (2022) 429–442.
- [55] S. Kumar, P. Kashyap, S. Chowdhury, S. Kumar, A. Panwar, A. Kumar, Identification of phytochemicals as potential therapeutic agents that binds to Nsp15 protein target of coronavirus (SARS-CoV-2) that are capable of inhibiting virus replication, *Phytomedicine* 85 (2021), 153317.
- [56] S. Thakal, A. Singh, V. Singh, In vitro and in silico evaluation of N-(alkyl/aryl)-2-chloro-4-nitro-5-[(4-nitrophenyl) sulfamoyl] benzamide derivatives for anti-diabetic potential using docking and molecular dynamic simulations, *J. Biomol. Struct. Dyn.* 40 (9) (2022) 4140–4163.
- [57] R. Shukla, T.R. Singh, High-throughput screening of natural compounds and inhibition of a major therapeutic target HsGSK-3 β for Alzheimer's disease using computational approaches, *J. Genetic Eng. Biotechnol.* 19 (1) (2021) 1–17.